JOURNAL OF MATERIALS SCIENCE 25 (1990) 1479–1486

Phase properties of the rapid cooled palladium–silicon alloy in the concentration range 40 to 58 at. % silicon

K. TSUMORI, H. AKIMUNE
Plasma Physics Laboratory, Kyoto University, Gokasho, Uji, Kyoto, 611, Japan

The phase diagram for the palladium–silicon system is reinvestigated by thermal analysis using a method taking the second derivative of time-dependent temperature and by metallographic measurement, where the cooling rate is about 140° C min^{-1}. The second derivative offers a sensitive and accurate means for thermal analysis with aid of a microcomputer. The phase diagram has no peak for PdSi. At silicon concentrations higher than 50 at. %, the alloy appears to be the eutectic for a composition of PdSi and Si, with the eutectic point at 895° C and 50 at. % Si, and at silicon concentrations lower than 50 at. %, the alloy appears to be the eutectic for Pd_2Si and PdSi, with the eutectic point at 886° C and about 48.5 at. % Si. The phase properties appear to be largely affected by the phase stability of PdSi in company with the departure from thermal equilibrium in the thermal analysis. The addition of small amounts of silver impurity causes the collapse of the PdSi phase and the alloy appears to be a eutectic of constitutions Pd_2Si and Si in the concentration range from 33 to 100 at. % silicon.

1. Introduction

The phase diagram for palladium–silicon system has been investigated by several authors [1–5], and the diagram over the full range of concentrations is represented in the literature by Hansen [6] and by Elliot [7]. Recently, detailed investigation on the phase of the alloy including the intermetallic compound PdSi has been made by measurements of magnetic susceptibility and metallography along with thermal analysis [5], where the experiments have been performed under a slow cooling rate. The significant difference between the previous and recent phase diagrams is that the distinct temperature peak relevant to PdSi in the earlier diagram does not appear in the recent one. In the previous diagram, furthermore, the binary alloy is a typical eutetic of Si and PdSi in the silicon concentration range from 50 to 100 at. %, while in the recent one, the alloy is the anomalous eutectic in that concentration range, and the peritectic property appears in silicon concentrations smaller than 50 at. %.

The crystallographic parameters of palladium–silicon intermetallic compounds have been investigated by several authors [8–10]. According to those investigations, the intermetallic compound Pd_2Si makes stable hexagonal structures in the solid phase, and the lattices of Si crystal and Pd_2Si can fit well, within 2% [11], so that if the alloy consisted of only dual constitutions of Pd_2Si and Si, it would be stable. On the other hand, PdSi is not so stable, especially at temperatures lower than 824° C Ω [5]; it is unstable and changes into the silicon-rich Pd_2Si and [5], so that in the concentration range where the alloy includes large amounts of PdSi, it is expected that the phase properties depend largely on the cooling rate. The phase properties may be also changed with small amounts of impurities which affect the phase stability of PdSi.

In this paper, the phase properties of the palladium–silicon system are reinvestigated in an attempt to examine the fundamental property relevant to a functional material which is applied to produce the negative hydrogen ion [12]. The requirements of the material are that the partial area of Si crystal fragments distributed on the material surface is ten per cent, that the rest of the constitution is permeable to hydrogen, and that the disc sliced from the ingot is airtight.

The Si concentrations in samples prepared for the experiment vary from 40 to 58 at. %; the values are in the range where the alloys include the PdSi compound. Thermal analysis along with metallographic measurements is made under a medium cooling rate of about 140° C min^{-1}; this value is about ten times larger than that obtained previously [5]. Investigation is also made of palladium silicide including a small amount of silver.

2. Experimental details

2.1. Apparatus

The apparatus is shown schematically in Fig. 1. The chamber is evacuated by a turbo molecular pump (TMP). The attainable base pressure without sample alloy is about 2×10^{-6} torr. In order to avoid the oxidation of the sample alloys, argon gas is supplied to the evacuated chamber through MnO filter (F), and flows out through a gas flow meter (FM).

The Al_2O_3 Tamman crucible (C), in which the sample alloy is loaded, is set on the graphite block (GB) supported by two fused quartz tubes (QT2, QT3). The heated region is shielded with a long fused quartz tube (QT1).

0022–2461/90 $03.00 + .12

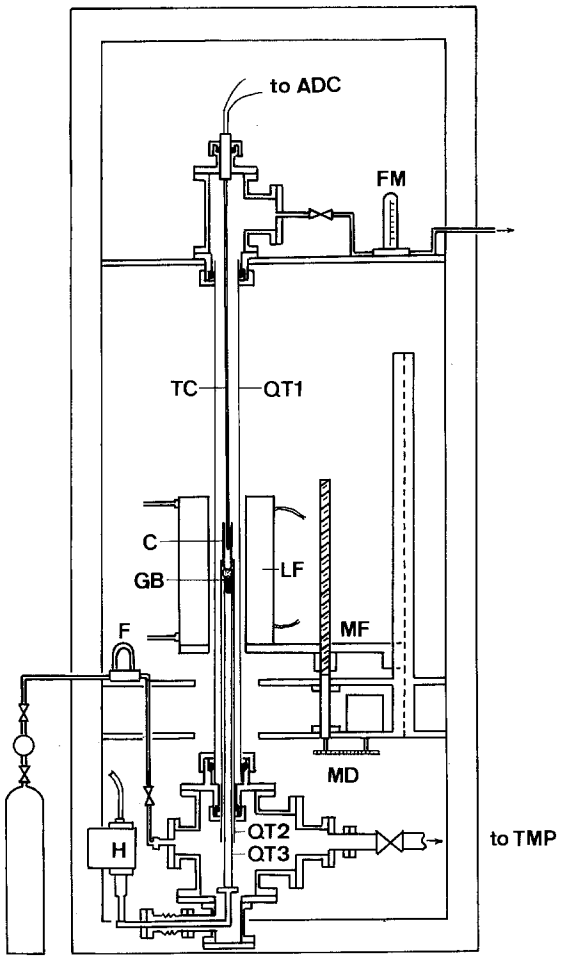

Figure 1 Apparatus for thermal analysis. ADC: analog/digital converter; FM: gas flow meter; TC: platinum/platinum–13% rhodium thermocouple; QT1, QT2 and QT3: fused quartz tubes; C: Al_2O_3 Tamman crucible; GB: graphite block; LF: water-cooled lamp furnace; F: MnO oxygen filter; MF: moving flame; MD: motor drive; H: ultrasonic homogenizer; TMP: turbo molecular pump.

The water-cooled lamp furnace (LF) is used for melting the sample; the furnace has a fairly small thermal inertia by nature, and is available to heat a 15 mm diameter sample up to 1500° C. The temperature distribution in the furnace is uniform over 140 mm length and decreases slightly near both open ends. The furnace is set on the moving flame (MF) and its position is adjustable with the motor drive (MD).

The thermodynamic characteristic temperatures, which are the liquidus and solidus temperatures, temperatures of invariant reactions and second order phase transition, are measured directly by the platinum/platinum–13% rhodium thermocouple (TC); the portion around the sensing point of the thermocouple is covered by a 0.2 mm-thick Al_2O_3 sheath to avoid the reaction of platinum with silicon. The thermocouple assembly is movable vertically to adjust the sensing point to any position of the sample alloys in liquid state. In order to reduce the influence due to the thermal inertia of the assembly, the total weight of the sensing portion is minimized, and its weight ratio to the sample is reduced to less than about 4 wt %. The ultrasonic homogenizer (H) is equipped in order to homogenize the sample in the liquid phase and to avoid super-cooling in the solidification of the sample.

2.2. Sample preparation

To avoid an explosive reaction of silicon with palladium, the PdSi compound (made by CERAC Inc.) was used as host material; its purity was 99.5%, and the rest comprised mostly the other phases of palladium silicide with composition of Pd : Si = 50.57 : 49.43 at. %. The main impurities of the powder were aluminium (0.1 at. %) and calcium (0.03 at. %). The samples of different compositions were made by addition of palladium metal (about 99.95% pure) and silicon lumps (about 99.9999% pure) to the host material.

The total weight of each sample alloy was about 25 g. The value was large compared with the weight of the Tamman crucible and the thermocouple assembly, and this could reduce the effect of thermal intertia from the other material.

The silicon concentration in the sample was estimated by weighing the initial materials before they were melted; the concentration was also estimated after solidification. Estimation was done using an image processor equipped with a microcomputer, which calculated the partial areas of the constitution in the image pattern through the metallograph. The silicon concentration in each sample was calculated from the partial areas using the numerical values of the sixth column in Table I and the ratio of composite atomic numbers corresponding to each constitution. The sample for the estimation was made of ingots which had been used for thermal analysis; the ingots were sliced by diamond ring saw horizontally into

TABLE I Crystallographic data of Pd-Si inter-metallic compounds and Si

Compounds	Crystal structures	Lattice parameters (Å)	Unit cell volume, V (Å^3)	Number atoms/unit cell, Z	Atomic volume, V/Z (Å^3)	Reference
Pd_2Si*	hexagonal	$a = 6.497$ $c = 3.432$	125.46	9	13.94	[8]
Pd_2Si'†	hexagonal super structure	$a + 2a_0 = 13.055$ $c = 8c_0 = 27.490$	4057.51	288	14.09	[9]
PdSi	orthorhombic	$a = 5.617$ $b = 3.391$ $c = 6.153$	117.21	8	14.65	[10]
Si	diamond cubic	$a = 5.430$	160.10	8	20.01	[13]

*Pd_2Si indicates 'silicon-poor Pd_2Si'
†Pd_2Si' indicates 'silicon-rich Pd_2Si'

many discs at regular intervals. the surface of each disc was polished successively finer and finally polished with 0.25 μm diamond paste, then measured by a metallograph under both direct and polarized lighting. The partial areas of silicon crystal and silicides on each surface were distinguished by a digital filter fitted to the image processor. The ratios of partial area corresponding to each constitution were averaged over all disc species sliced from the same ingot, because a small difference was seen between the ratios for the upper and lower discs. The silicon concentrations calculated from the averaged ratio agreed well with the values estimated from the initial materials.

2.3. Experimental procedure and data processing

Sample alloys of all Si concentrations were crushed into pieces, of probable diameters 0.1 mm, and loaded into a Al_2O_3 Tamman crucible. The attainable base pressure was about 3×10^{-6} torr after baking at about 700° C. The sample alloy was remelted in an argon atmosphere, where the argon gas flow rate was 100 $cm^3 min^{-1}$. The thermocouple assembly was moved down to the centre of the sample after melting. The temperature of the sample was held at 1400° C, and it was homogenized using an ultrasonic homogenizer to avoid separation of the components. In order to investigate the phase diagram for the Pd–Si system at medium cooling rate, the power to the lamp furnace was turned off after homogenization.

The time-dependent e.m.f. of the thermocouple was amplified by a pre-amplifier, converted into digital signals by an analog/digital converter (ADC), and stored in a microcomputer. The duration for a single measurement was 330 sec, the temperature of the sample alloy decreased from 1350° C to about 600° C in this time scale, where the sampling time was about 30 msec.

The dependences of the thermocouple e.m.f. on real temperatures were represented by a bicubic function with sufficient accuracy. In order to measure exactly all the thermodynamic characteristic temperatures, the second derivative of temperature with respect to time, d^2T/dt^2 was calculated numerically. The calculation was made successively with assigning the cubic functions best fitted to the time dependent $T(t)$ curve, during the short time interval which was taken as the signal to the digital noise ratio, maximized by the least squares method. The temperatures, at which the second derivative exhibited the peak, were automatically indicated as numerical values by computer programming.

The accuracy of the bicubic function was examined where the thermal analyses on silver and copper metals (99.99%) were made under the same conditions as the practical analysis for Pd–Si alloy. The melting temperatures of both metals agreed with well-known values to within 0.5° C, and the $T(t)$ curves were also found to be reasonable with reference to their phase diagrams.

3. Results and discussion

The phase diagram is derived from the temperatures at which the second derivative has a peak. Typical couples of $T(t)$ and the second derivative are shown in Figs 2a to c, which represent the computer processed curves for samples of 40, 50 and 58 at. % Si, respectively. In each figure, the vertical dashes below the temperature curves, which are automatically drawn by computer programming, indicate peak positions. The second derivatives are amplified by the same factor, 1.5 for all graphs; the noises in their curves may be due to the local fluctuation caused by the heterogeneous quality of the samples, indeed, when the silver or copper metals are measured, the noises become smaller.

In Fig. 2a, the first peak corresponds to the liquidus point of Pd_2Si, and the small second peak may relate to the invariant reaction in the liquid phase; the reaction is pointed out in Ref. [5] and is discussed later. The third peak indicates the initiation of solidification and the negative peak in the fourth sequence indicates the end of solidification. The last small negative peak may indicate that the second order phase transition occurs in the solid state.

In Fig. 2b, both curves behave in a simple manner and the last negative peak of the second derivative becomes distinguishable. This indicates that the 50 at. % Si sample makes a uniform PdSi alloy, and the PdSi alloy may change its structure immediately after the solidification.

In Fig. 2c, representing the characteristic curves for the 58 at. % Si sample, the first peak appears before the solidification and indicates the liquidus point of silicon. The negative peak just following the solidification peak is due to weak supercooling. When the supercooling takes place, the eutectic temperature is assigned to the point of the negative peak, because when supercooling takes place, the initiating temperature of solidification must be somewhat smaller than the exact eutectic temperature.

The typical structures seen through a metallograph are represented in Figs 3a to c. Fig. 3a shows the metallograph of 40 at. % Si alloy, where the white domain corresponds to Pd_2Si crystal and the dark grey area to PdSi matrix. The Pd_2Si crystals appear to make hexagonal structures. Furthermore, Pd_2Si crystals and PdSi matrix appear to make large composite hexagonal patterns. Indeed, a feature of the local structure appearing on the surface of the sample ingot has a hexagonal columnar form like quartz crystal.

Fig. 3b shows the enlarged metallograph of 50 at. % Si alloy. The grey matrix constitution is PdSi, where clusters of tiny silicon crystals appear, but the number density of the cluster is very small. All these clusters have tear-drop-like form, and are sprinkled on the surface of the sample disc.

Fig. 3c shows the metallograph of 58 at. % Si alloy, where massive silicon crystals of dark grey exist in the matrix of PdSi, and they orient in random directions in all areas of the sample disc. Most of the silicon crystals are separated into two parallel long domains by PdSi, and many cracks are seen over the surface. Their number seems to increase with silicon concentration in the alloy. The occurrence of cracking may be caused by a large lattice misfit and the difference in the thermal expansions between Si and PdSi crystals.

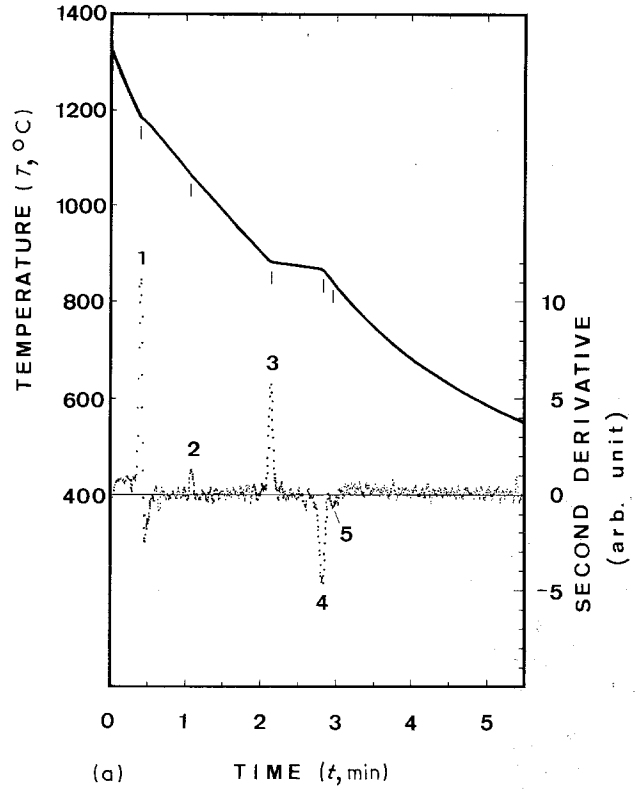

Figure 2 Typical time-dependent temperature curves, $T(t)$, and the second derivative of temperature, d^2T/dt^2 in thermal analysis of palladium–silicon binary alloys. (a) Behaviour of $T(t)$ and d^2T/dt^2 for the alloy of silicon concentration 40 at. %. Peak 1, T = 1184° C, liquidus temperature of Pd_2Si; peak 2, T = 1062° C, invariant reaction that $Pd_2Si + \delta PdSi$ or $Pd_2Si + \delta Si \rightarrow Pd_2Si'$; peak 3, T = 883° C, eutectic temperature; peak 4, T = 864° C, end of solidification; peak 5, T = 843° C, second order phase transition in solid state. (b) Behaviour of $T(t)$ and d^2T/dt^2 for the alloy of silicon concentration 50 at. %. Peak 1, T = 897° C, eutectic temperature; peak 2, T = 880° C, end of solidification; peak 3, T = 835° C, second order phase transition in solid state. (c) Behaviour of $T(t)$ and d^2T/dt^2 for the alloy of silicon concentration 58 at. %. Peak 1, T = 1038° C, liquidus temperature of silicon; peak 2, T = 892° C, initiating temperature of solidification under a slight supercooling; peak 3, 894° C, real eutectic temperature; peak 4, T = 878° C, end of solidification; peak 5, T = 811° C, second order phase transition in solid state.

Fig. 4 represents the phase diagram estimated from thermal analysis and the metallography. Plots on the diagram are obtained from experiments on 23 ingots, where in all cases, the weight of each ingot is about 25 g and the cooling rate is about 140° C min^{-1}. The thermal analysis is repeated several times for the sampled ingots over the temperature range from 1350° C to 600° C. The repetition shows that the characteristic temperatures are valid with every trial, though the peak amplitudes of the second derivative fluctuate by each trial.

In Fig. 4, the characteristic point at 48.5 at. % Si and 886° C is given as a point where extension of the falling gradient line crosses the horizontal line at 886° C, taking account of experimental plots existing to the right of the point. The vertical line at 50 at. % Si, which indicates a phase boundary, is decided mainly by metallographic measurements. The constitution of just 50 at. % Si alloy appears to be homogeneous PdSi, and even at silicon concentrations slightly smaller than this value, both constitutions Pd_2Si and PdSi appear in heterogeneous form, whereas at slightly higher concentrations, PdSi and Si crystals appear in heterogeneous form. Moreover, the second derivative curve of thermal analysis exhibits a simple form for 50 at. % Si alloy, and for shifted concentration additional peaks appear on the curve. The global feature of the diagram is similar only in form, to the diagram for the full concentration range of the gold–antimony alloy [14].

Fig. 4 shows that the characteristic temperature of 50 at. % Si alloy does not exhibit a peak value as represented in literature by Hansen [6], but appears to

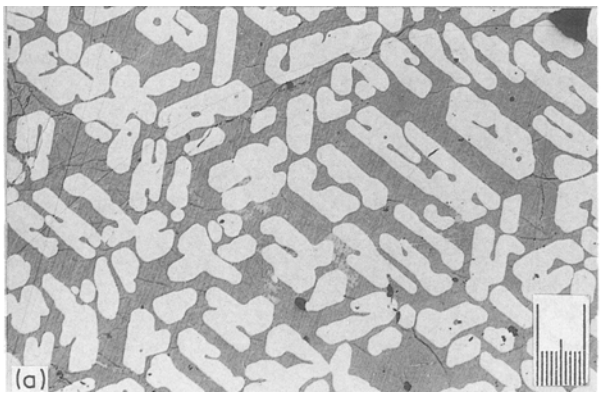

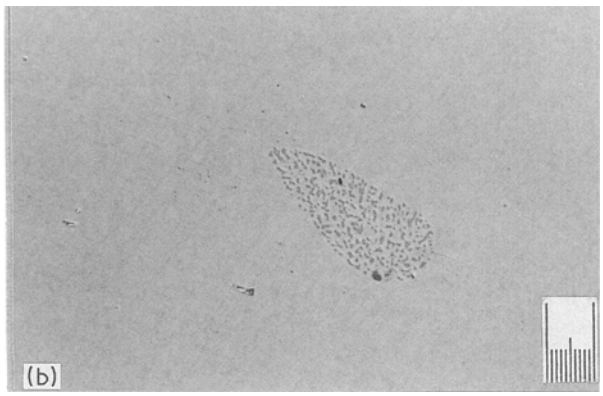

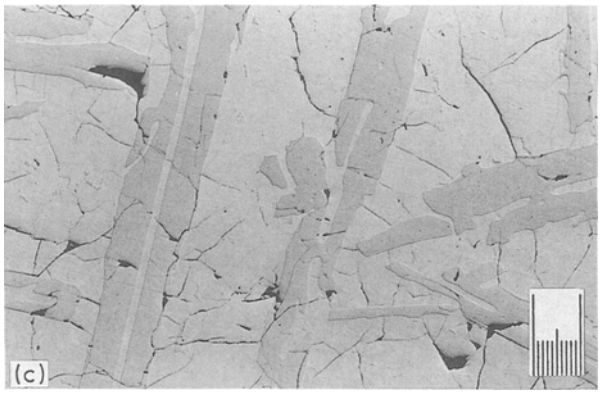

Figure 3 Metallographs of palladium–silicon binary alloys of different silicon concentrations. (a) Metallograph for the alloy of silicon concentration 40 at. %. Hexagonal-like white areas are Pd_2Si crystals and dark grey area is the PdSi matrix. The scale is 100 μm. (b) Metallograph for the alloy of silicon concentration 50 at. %. Grey area is PdSi matrix and dark grey dots in cluster are small silicon crystals. The scale is 10 μm. (c) Metallograph for the alloy of silicon concentration 58 at. %. Dark grey areas are silicon crystals and grey area is PdSi matrix. The scale is 100 μm.

be equal to the solidus temperature; the same evidence is also given by Langer and Wachtel [5], although differences exist in the detailed properties.

The phase diagram in Fig. 4 is divided into two sections with respect to silicon concentration. In the silicon concentration range of 50 to 60 at. %, the alloy appears to be the eutectic relating to PdSi and Si. The eutectic point just coincides with the solidus temperature of PdSi, so that in decreasing the temperature, all excess silicon in the liquid phase is solidified as primary crystal until the eutectic temperature is attained. The situation causes the alloy to grow to the massive silicon crystals as shown in Fig. 3c, even with comparatively rapid cooling rate. When the PdSi alloy including a very small excess of Si is made, solidification takes place at the eutectic temperature, so that the fragmented silicon crystals appear as small cluster feature as shown in Fig. 3b.

In the silicon concentration range of 40 to 50 at. %, the phase diagram, on the whole, appears to be a binary alloy of Pd_2Si and PdSi, and the eutectic point is 48.5 at. % of Si and 886° C. The horizontal line at 1063° C appears to be caused by an invariant reaction in the liquid phase; the reaction may be

$$Pd_2Si + \delta PdSi \rightarrow Pd_2Si' \quad \text{or} \quad Pd_2Si + \delta Si \rightarrow Pd_2Si'$$

where δPdSi and δSi denote small amounts of PdSi and Si, respectively, and Pd_2Si' denotes silicon-rich Pd_2Si following Langer and Wachtel [5]. However, Pd_2Si and Pd_2Si' cannot be identified by metallographic measurements. The metallograph of an alloy of 46 at. % Si, which is near to the eutectic concentration, shows that there exist small amounts of fine Pd_2Si or Pd_2Si' along with their massive crystals, although such a fine structure is not observed for an alloy including sufficiently less silicon, as seen in Fig. 3a. The facts appear to show that the fine Pd_2Si or Pd_2Si' structure is made by solidification at the eutectic temperature.

The plots appearing below the eutectic temperature are divided into two groups; plots in the silicon concentration range of 40 to 45 at. % align almost on a line of 845° C, while plots at a higher concentration range are scattered. The mean temperature of scattered plots is 831° C, and the dispersion in temperature evaluated

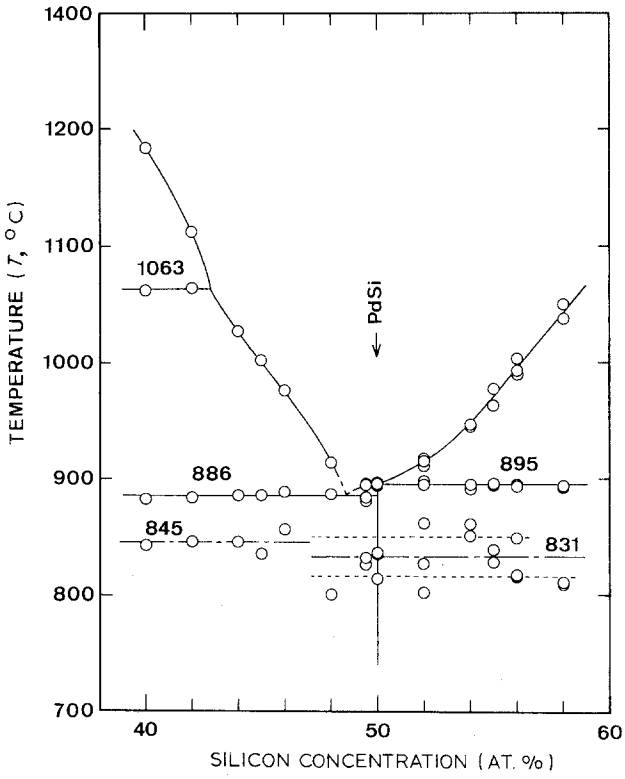

Figure 4 Phase diagram of palladium–silicon system obtained under medium cooling rate. Dashed lines represent extension from the experimental lines, two straight dot-dashed lines (—·—) are the mean temperatures of second order phase transition in solid state, and two straight dotted lines (· · · ·) represent the temperature dispersion assuming Gaussian distribution of experimental plots.

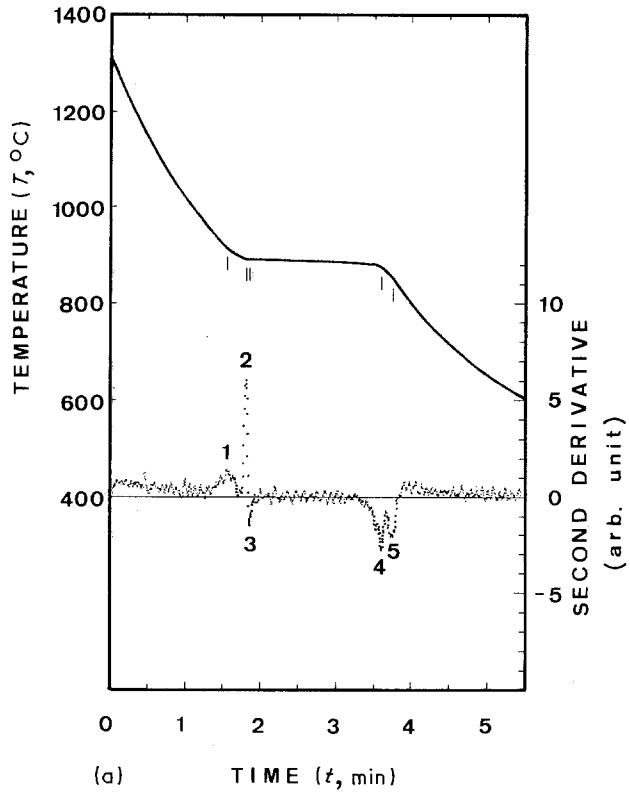

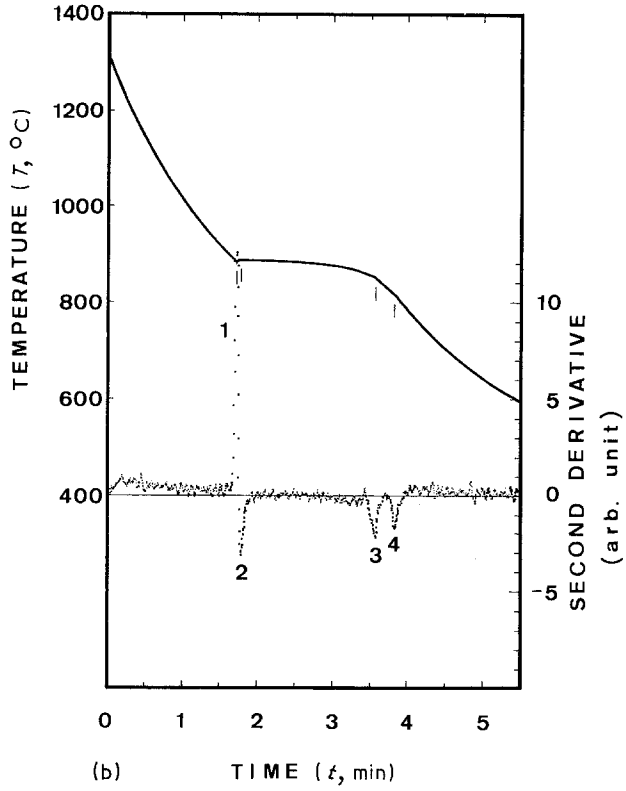

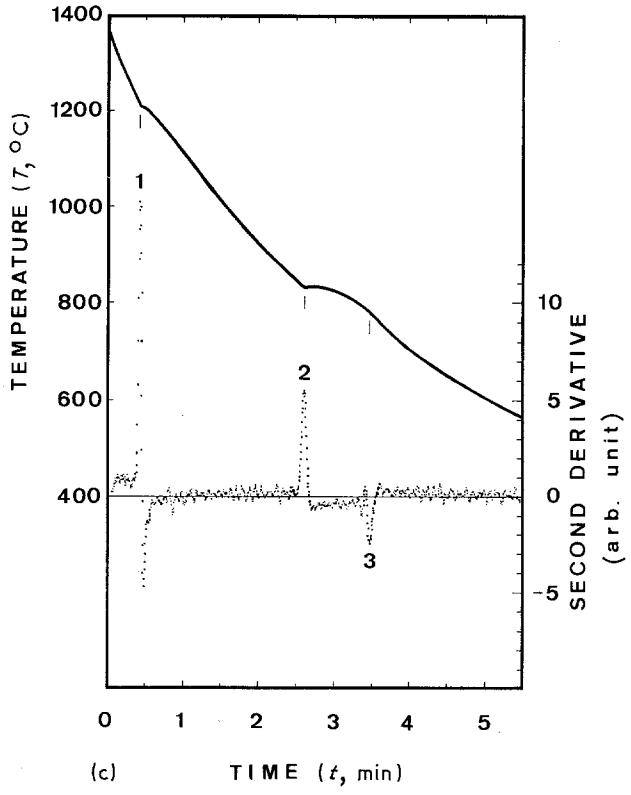

Figure 5 Time-dependent temperature curves, $T(t)$, and the second derivative of temperature, d^2T/dt^2 for palladium–silicon alloy with and without silver impurity. (a) Behaviour of $T(t)$ and d^2T/dt^2 for the Pd–Si alloy; atomic concentration ratio is Pd : Si = 48 : 52 and Pd : Ag = 100 : 0. Peak 1, T = 916° C, liquidus temperature of silicon; peak 2, T = 893° C, initiating temperature of solidification under a slight supercooling; peak 3, T = 894° C, real eutectic temperature; peak 4, T = 876° C, end of solidification; peak 5, T = 851° C, second order phase transition in solid state. (b) Behaviour of $T(t)$ and d^2T/dt^2 for the Pd–Si alloy; atomic concentration ratio is Pd : Si = 48 : 52 and Pd : Ag = 98 : 2. Peak 1, T = 884° C, initiating temperature of solidification under supercooling; peak 2, T = 888° C, real eutectic temperature; peak 3, T = 850° C, end of solidification; peak 4, T = 815° C, second order phase transition in solid state. (c) Behaviour of $T(t)$ and d^2T/dt^2 for the Pd–Si alloy; atomic concentration ratio is that Pd : Si = 60 : 40 and Pd : Ag = 92 : 8. Peak 1, T = 1210° C, liquidus temperature of Pd_2Si; peak 2, T = 833° C, eutectic temperature; peak 3, T = 782° C, end of solidification.

assuming the Gaussian distribution is 848° C and 814° C. Langer and Wachtel [5] describe the invariant reaction for PdSi to change into Pd_2Si' and Si as taking place near these temperatures. However, the reaction is unlikely to occur at a temperature higher than 824° C. Moreover, even in the temperature range below 824° C, the reaction is moderate. On the basis of these facts, the plots seem to correspond to second order phase transition in the solid state.

The second order phase transition may be the transition of the lattice structure of PdSi to the orthorhombic which is the stable lattice structure of PdSi at the room temperature. The reason why the plots do not scatter in the low silicon concentration range and do in the higher concentration is not clear. A plausible explanation is as follows. At low concentrations of silicon, PdSi and Pd_2Si form the hexagonal structure in a lump as seen in Fig. 3a, so that PdSi may be constricted by the ambient massive Pd_2Si, and the transition to the orthorhombic structure may take place at a temperature slightly higher than that at high silicon concentration. On the other hand, at high silicon concentrations, the primary crystals of silicon grow in a random manner as seen in Fig. 3c, so that they may not impose stress field on PdSi in the solid phase, and some margin in lattice formation may give uncertainty in the transition along with lowering the mean transition temperature. Even in a silicon concentration somewhat lower than 50 at. %, the plots are scattered. That fact may be caused by the absence of a strong stress field on PdSi in the solid phase, because the size of each primary crystal of Pd_2Si is small and

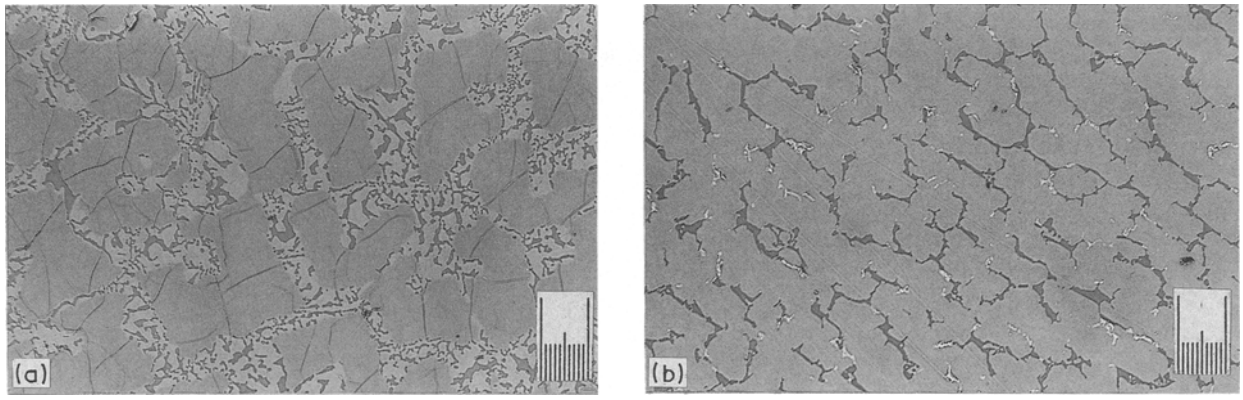

Figure 6 Metallographs of palladium–silicon alloy including silver impurity. (a) Metallograph for the Pd–Si alloy; atomic concentration ratio is Pd : Si = 48 : 52 and Pd : Ag = 98 : 2. Medium grey area is PdSi, light grey area is Pd_2Si and fragmented dark grey portions are silicon crystals. The scale is 50 μm. (b) Metallograph for the Pd–Si alloy; atomic concentration ratio is Pd : Si = 60 : 40 and Pd : Ag = 92 : 8. Light grey area is Pd_2Si and dark grey portions are Si crystals. Silver precipitates at the pointed ends of silicon crystals. The scale is 50 μm.

the lumped hexagonal structure does not appear at a silicon concentration somewhat lower than 50 at. %.

In comparison with the phase diagram given by Langer and Wachtel [5], there are some differences in form in the vicinity of the two eutectic points. The diagram in Fig. 4 has the temperature minimum at a silicon concentration of 2 at. % lower than 50 at. % and appears to be the eutectic point of Pd_2Si and PdSi, while the characteristic temperature at a silicon concentration of 50 at. % appears to be the eutectic point of PdSi and Si. On the other hand, the diagram given by Langer and Wachtel [5] has the temperature minimum at a silicon concentration 2 at. % higher than 50 at. % and is the anomalous eutectic point of PdSi and Si, while the characteristic temperature at a silicon concentration of 50 at. % is only the liquidus point of Pd_2Si'.

The origin of these differences is not clear, but the important source is supposed to relate the phase stability of PdSi along with a difference in the cooling rate in both experiments. A qualitative explanation for the source is as follows. At a liquidus temperature of Pd_2Si in silicon-poor concentration, the interaction between PdSi and Pd_2Si may be weakly repulsive, but some PdSi is probably included in the Pd_2Si phase, and silicon-rich Pd_2Si, that is Pd_2Si', is formed. The amount of included PdSi depends on the cooling rate and tends to decrease with the cooling rate. This tendency may give rise to the eutectic property of PdSi and Pd_2Si in a silicon-poor concentration as seen in this experiment.

Figs 5a and b represent $T(t)$ and its second derivative for 52 at. % Si alloys, where Fig. 5b represents both curves for the alloy containing 2 at. % Ag with respect to the palladium concentration. The alloy without silver exhibits peak 1 relevant to the liquidus temperature, where the silicon primary crystal grows, while the alloy containing silver does not exhibit the peak, and the d^2T/dt^2 curve becomes simple. Fig. 5c represents both curves for 40 at. % Si alloy containing 8 at. % Ag with respect to the palladium concentration. The second derivative peak relevant to the invariant reaction in the liquid phase disappears, and also the peak relevant to the second order phase transition of PdSi in the solid state disappears in contrast with fact that they exist in Fig. 2a. In general, the comparison of second derivatives for alloys with and without silver indicates that the addition of small amounts of silver leads to an appreciable change in properties of the phase diagram.

Fig. 6a represents the metallograph of 52 at. % Si alloy containing 2 at. % Ag with respect to the palladium concentration, where the medium grey area shows PdSi, the light grey area indicates Pd_2Si or Pd_2Si', and the dark grey fragments are Si crystals. When the silver content increases up to about 8 at. % with respect to the palladium concentration, the whole surface of the disc becomes silicon crystal fragments and Pd_2Si or Pd_2Si'. Fig. 6b is a metallograph of the alloy corresponding to Fig. 5c, where the concentration ratio is Pd : Si = 60 : 40 and Pd : Ag = 92 : 8. The light grey area is probably Pd_2Si, the dark grey areas are silicon crystal fragments, and the precipitating silver is shown as small white areas which terminate the pointed end of the Si crystals, and the cracks disappear completely.

The investigations of thermal analysis and metallography for the wide range of silicon concentrations indicate that the addition of a small amount of silver collapses PdSi and separates the system into the binary constitution of Pd_2Si and Si [15]. Consequently, the phase diagram comes to behave as the eutectic alloy of Pd_2Si and Si.

4. Conclusion

The phase properties of the palladium–silicon system are reinvestigated by thermal analysis and metallographic measurement in an attempt to obtain a functional material which consists of dual constitutions; those are fragmented silicon crystals and substances permeable to hydrogen.

In thermal analysis, the method of taking the second derivative of the time-dependent temperature curve offers a sensitive and accurate means to detect and read the thermodynamic characteristic temperatures of the Pd–Si alloy, providing that the heat capacity of the sample alloy is large enough compared with those of the equipment, and that a suitable

procedure using a microcomputer is applied to processing the measured values.

The phase diagram obtained over the silicon concentration range from 40 to 58 at. % under the medium cooling rate of 140° C min^{-1} shows that the liquidus temperature relevant to the inter-metallic compound PdSi has no peak in the diagram. In that silicon concentration range, the phase diagram appears to be divisible into two sections; at silicon concentrations of 40 to 50 at. %, the alloy is a eutectic of Pd_2Si and PdSi, and at silicon concentrations from 50 to 58 at. %, the alloy is also the eutectic of PdSi and Si. The alloy of sufficiently poor silicon concentration has a heterogeneous hexagonal pattern consisting of Pd_2Si and PdSi. The 50 at. % Si alloy is almost a single constitution of PdSi. The alloy of sufficiently rich silicon concentration consists of PdSi and random fractions of the primary Si crystal, and has many cracks.

The addition of a certain amount of silver collapses PdSi, and the silicide forms dual constitutions of Pd_2Si and fragmented Si crystals. In this alloy, a little precipitated silver can be seen on the surface of the sliced disc, and cracks do not exist.

Acknowledgement

The authors would like to express our thanks to Professor M. Yamaguchi of the Department of Metal Science and Technology of Kyoto University for his helpful and valuable discussions. The authors would also like to express our thanks to Mr S. Tamura, Dr T. Sakai and Mr T. Soshiroda of Kobe Steel Ltd for their kind advice.

References

1. P. LEBEAU and P. JOLIBOIS, *Compt. Rend.* **146** (1908) 1028.
2. A. T. GRIGOEV, T. A. STRUINA and A. S. ADAOVA, *Izvest. Sektora Platiny* **27** (1952) 219.
3. N. K. RAO and H. WINTERHAGER, *Trans. Indian Inst. Metals* **10** (1956–1957) 139.
4. E. ROSCHEL and C. J. ROUB, *Z. Metallkde* **62** (1971) 840.
5. H. LANGER and E. WACHTEL, *Z. Metallkde* **72** (1981) 769.
6. P. M. HANSEN, in "Constitution of Binary Alloys" (McGraw-Hill, New York, 1958) pp. 1125–1201.
7. R. P. ELLIOT, in "Constitution of Binary Alloys, First Supplement" (McGraw-Hill, New York, 1965) pp. 731–2.
8. B. ARONSSON and A. NYLUND, *Acta Chem. Scand.* **14** (1960) 1011.
9. A. NYLUND, *Acta Chem. Scand.* **20** (1966) 2381.
10. I. ENGSTRÖM, *Acta Chem. Scand.* **24** (1970) 1466.
11. W. D. BUCKLEY and S. C. MOSS, *Solid-State Electron.* **15** (1971) 1331.
12. H. AKIMUNE, *J. Appl. Phys.* **54** (1983) 18.
13. C. KITTEL, in "Introduction to Solid State Physics", 5th Edn (John Wiley and Sons, New York, 1976) pp. 31–2.
14. R. VOGEL, *Z. Anorg. Chem.* **50** (1906) 151.
15. K. TSUMORI and H. AKIMUNE, to be published.

Received 20 October 1988
and accepted 14 April 1989